NeuroImage **17,** 967–976 (2002)
doi:10.1006/nimg.2002.1172

Fast, Fully Automated Global and Local Magnetic Field Optimization for fMRI of the Human Brain

James L. Wilson,* Mark Jenkinson,* Ivan de Araujo,† Morten L. Kringelbach,† Edmund T. Rolls,† and Peter Jezzard*,[1]

*Centre for Functional Magnetic Resonance Imaging of the Brain, University of Oxford, John Radcliffe Hospital, Oxford OX3 9DU, United Kingdom; and †Department of Experimental Psychology, University of Oxford, South Parks Road, Oxford OX1 3UD, United Kingdom

Received December 4, 2001

The aim of this novel technique is to allow researchers, particularly those operating at high static magnetic field strengths on fMRI applications, to tailor the static magnetic field within the brain. The optimum solution for their experimental needs is reached, utilizing the full potential of the active shims at their disposal. The method for shimming human brain, which incorporates automatic brain segmentation to remove nonbrain tissue from the optimization routine, is presented and validated. The technique is fast, robust, and accurate, achieving the global minimum to a static field homogeneity function of the *in vivo* brain. Both global and specified local regions of the brain can be selected on which to optimize the shims without requiring skilled intervention. The effectiveness of the automated local shim is demonstrated in an olfactory fMRI study where significant activations in the orbitofrontal cortex were very clear when the above method was employed.

Key Words: **automatic shimming; fMRI; magnetic field homogeneity; susceptibility artifacts; olfaction.**

INTRODUCTION

With experiments performed at ever higher static magnetic field (B_0) strengths, the optimization of *in vivo* shimming techniques is critical for applications such as functional MRI (fMRI) (Jezzard and Clare, 1999) and MR spectroscopic imaging (Spielman *et al.*, 1998). Subject-specific geometric and magnetic susceptibility variations within the human head lead to local distortions in the B_0 field within the brain (Ericsson *et al.*, 1995; Li *et al.*, 1996) particularly in the vicinity of air–tissue interfaces (e.g., superior to the sphenoid/ethmoid sinus and the mastoid air cells) where susceptibility differences of 9.5 parts per million (ppm) exist (Li *et al.*, 1996). The rapid imaging methods used in fMRI, namely echo planar imaging (EPI) and spiral methods, are particularly vulnerable to the resulting susceptibility artifacts of geometric distortion and localised signal loss (Ojemann *et al.*, 1997). Automated shimming techniques, applied on a subject-by-subject basis, have long been used to reduce susceptibility artifacts by minimizing the low spatial frequency components of B_0 inhomogeneity. The motivation for this study was to develop an improved automated method of shimming the human brain for use in high field fMRI.

The simplest automated shimming techniques use optimization strategies, such as the simplex method (Nelder and Mead, 1965), to maximize the free induction decay (FID) signal (Holz *et al.*, 1988). Field mapping techniques are a more time efficient approach that, unlike the simplex method, can obtain the global B_0 homogeneity solution. Of these, phase mapping approaches (Prammer *et al.*, 1988; Webb and Macovski, 1991; Schneider and Glover, 1991; Wen and Jaffer, 1995) have typical run times of 3 to 10 min but can suffer from poor lipid suppression, particularly at higher field stengths. The run time can be substantially decreased by either utilizing an EPI sequence (Reese *et al.*, 1995) or mapping the B_0 field along a small number of linear projections (Gruetter, 1993). Spectroscopic methods (Mackenzie *et al.*, 1987; Tropp *et al.*, 1989; Hu *et al.*, 1995) are free from chemical shift artifact but take substantially longer to acquire. To date all automated shimming methods have optimized the B_0 field distribution within a manually defined or signal intensity thresholded region of interest (ROI).

Here, we present a robust, fully operator-independent shimming technique that runs in under 80 s, denoted the "brain shim." Although based on previous phase mapping approaches (Prammer *et al.*, 1988; Webb and Macovski, 1991; Schneider and Glover, 1991; Wen and Jaffer, 1995), we perform a novel brain segmentation step enabling shim optimization of the *in*

[1] To whom correspondence should be addressed. Fax: +44 [0]1865 222717. E-mail: peterj@fmrib.ox.ac.uk.

1053-8119/02 $35.00

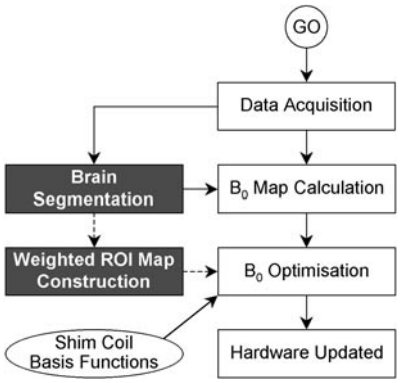

FIG. 1. Overview of the brain shim procedure. Steps that are novel to this technique are highlighted. A weighted ROI map is constructed only for use in local shimming.

vivo brain without surrounding structures. Fully automated "local shimming" of the brain was integrated as part of the technique by preferentially weighting specified regions of the brain. This extension allows the experimenter to tailor the resultant static field within the brain to fit experimental interests. To show the usefulness of the technique an olfactory fMRI study of the inferior frontal lobe of the brain, which experiences large susceptibility artifacts, was conducted utilizing brain shim and local shim techniques.

THEORY

An overview of the brain shim procedure is shown in Fig. 1. Details on each step performed after data acquisition are provided in this section. All steps are fully automated. To perform local brain shimming, weighting factors are inputted prior to shim run commencement, e.g., as part of a predefined scan protocol.

Brain Segmentation

Nonbrain tissue, namely subcutaneous fat, bone marrow, and in particular tissue found inferior to the frontal and temporal lobes—muscles, tendons, and sinus regions (through partial voluming effects)—as well as ocular components, are often highly off-resonance and not of direct interest. To remove the confounding effect of such regions on the shim optimization algorithm we derive an *in vivo* brain mask that defines our volume of interest (VOI). This is a four-step process. The first step is to acquire a representative reference head data set, R, and manually create a reference brain mask (R_B). This step is performed only once and the results are stored as a reference on disk. For all subsequent brain shim procedures, following the acquisition of data, step two is to reconstruct the individual subject's head image, S, by taking the magnitude-reconstructed field map data set. Third, a transformation matrix, $\mathbf{T}$, is derived that registers S to R (i.e., $R = \mathbf{T}S$) using a 12-parameter affine registration algorithm (Jenkinson and Smith, 2001, source code available from http://www.fmrib.ox.ac.uk/fsl/). Finally, the *in vivo* brain mask, S_B, is generated through $S_B = \mathbf{T}^{-1}R_B$ and identifies the VOI for B_0 map calculation.

B_0 Map Calculation

The B_0 map is constructed in a similar fashion to a previous study (Wen and Jaffer, 1995). However, we utilize a novel, fast, and automatic phase unwrapping algorithm[2] that starts by segmenting the image into areas within which the phase variation is small. The areas are progressively merged, adding appropriate 2π offsets where required, until the merged area covers the entire VOI. Choosing which areas to merge is based on a cost function that measures the sum of square phase differences over the boundary separating the areas.

Weighted ROI Map Construction

The intersubject variation in the location of the inferior frontal and inferior temporal B_0 inhomogeneities in a nine-subject sample was found to be approximately 3 mm (see Appendix A). The spatial distribution of large B_0 inhomogeneities is thus relatively consistent between subjects.

Following the above study we define, and store on disk, five ROIs in our reference brain as shown in Fig. 2a. These regions were operationally defined with reference to a typical B_0 field map of the brain in order to reflect the main B_0 inhomogeneous regions of the brain. Figures 2a and 2b demonstrate that each ROI corresponds to an area of similar shim characteristic. The inferior frontal and inferior temporal ROIs contain large B_0 inhomogeneities; the cerebellum ROI is anatomically defined; the superior frontal ROI is susceptible to substantial off-resonance effects; the posterior ROI covers the remainder of the brain and is thus devoid of highly off-resonance areas. The inferior frontal, inferior temporal, and cerebellum regions we collectively name the inferior ROIs. The choice of more optimal ROI definitions may allow for minor improvements in the target function of specific regions.

To perform fully automated local shimming of the brain a weighted ROI map, R_W, is constructed from inputted weighting parameters predefined as part of the scan protocol, transformed into an *in vivo* weighted ROI map, S_W, through $S_W = \mathbf{T}^{-1}R_W$ and spatially smoothed with a $3 \times 3 \times 3$ voxel kernel to remove abrupt changes in weighting value. S_W is then used to

[2] Jenkinson, M. (2001). A fast, automated, *n*-dimensional 3D phase unwrapping algorithm (PRELUDE). FMRIB Technical Report TR01MJ1, FMRIB Centre, University of Oxford. Documentation available from http://www.fmrib.ox.ac.uk/analysis/; source code available as a component of FUGUE from http://www.fmrib.ox.ac.uk/fsl/.

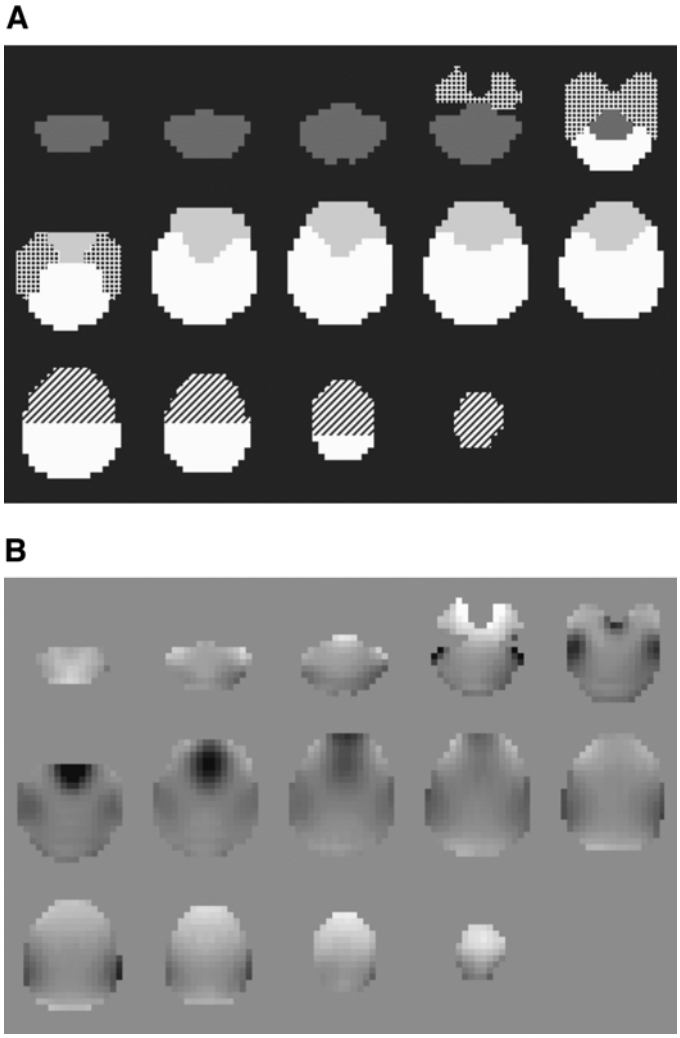

FIG. 2. (A) The five defined ROIs of the reference brain: (▨) superior frontal; (▩) inferior frontal; (▤) inferior temporal; (■) cerebellar; (□) posterior. Each region corresponds to an area of similar shim characteristic. (B) A typical postmanual shim, low-resolution B_0 field map of the reference brain with a gray scale of 150 Hz for the full range.

spatially weight the optimization target function (as shown subsequently in Eq. (1)).

Weighting parameters are chosen by the researcher prior to scanning as part of a predefined scan protocol and indicate which brain regions are of particular or preferential interest; these weights are therefore independent of both operator and subject. For example, an fMRI study of the orbitofrontal cortex performed on a group of volunteers may demand a weighting of unity in the inferior frontal ROI and zero elsewhere. The same weighting parameters are applied to each subject. It is also possible to utilize an additional, researcher-defined ROI for local shimming, derived either in the reference brain prior to scanning (then incorporated into R_W) or in the *in vivo* brain during scanning (then incorporated directly into S_W).

B_0 Optimization

To optimize the static magnetic field, a homogeneity target function must be minimized with knowledge of the *in vivo* B_0 variation, the shim coil basis functions, and, if required, a weighted ROI map. Once the optimal shim coil currents are determined, the input to the shim coil amplifiers is updated and the scanner resonance frequency adjusted using a pulse-acquire sequence.

The implementation used in the present study utilizes a shim current constrained algorithm (Wen and Jaffer, 1995), with the modification of a conventional least-squares target function (Prammer *et al.*, 1988; Webb and Macovski, 1991; Schneider and Glover, 1991; Reese *et al.*, 1995; Mackenzie *et al.*, 1987; Tropp *et al.*, 1989; Hu *et al.*, 1995), L, defined as

$$L = \sqrt{\sum_{\mathrm{VOI}} S_W(B_0(x, y, z) - \langle B_0 \rangle)^2}, \qquad (1)$$

where $\langle B_0 \rangle$ is the average static field within the VOI. S_W is equal to unity at all points in space for global brain shimming. Practically, the minimization of this target function has the effect of placing the VOI as close to resonance as possible, so reducing spatial distortion effects. An additional B_0 homogeneity measure used in the analysis of our results, D (Wen and Jaffer, 1995), is effectively a measure of local signal loss artifact and is defined as

$$D = \sqrt{\sum_{\mathrm{VOI}} \left[\left(\frac{\partial B_0}{\partial x} \right)^2 L_x^2 + \left(\frac{\partial B_0}{\partial y} \right)^2 L_y^2 + \left(\frac{\partial B_0}{\partial z} \right)^2 L_z^2 \right]}, \qquad (2)$$

where L_x, L_y, L_z are the voxel dimensions to be used in the imaging study. To obtain this expression, the first-order intervoxel field derivatives have replaced the true intravoxel field variations as a measure of intravoxel dephasing. This is reasonable as long as the voxel dimensions in the field map are not large.

MATERIALS AND METHODS

All experiments were performed on a 3-T Varian Inova spectrometer fitted with a quadrature birdcage head coil. Five second-order room temperature shim terms were supplied via an Oxford shim power supply (Type 2358) attached to a (otherwise disconnected) Siemens AS25 whole-body gradient coil. First-order shim terms were implemented as current offsets to a Magnex SGRAD head gradient coil, housed within the Siemens coil. The linear shims, the z^2 shim, and the remaining quadratic shims generated maximum field offsets of 6.9, 6.2, and 1.0 ppm, respectively, on the surface of a 20-cm-diameter sphere placed at the mag-

net's isocenter. All brain shim computation was run on the console computer, a Sun Blade 1000.

The field mapping sequence was an axial symmetric–asymmetric multislice spin-echo acquisition with parameters: data matrix = 32 × 32, 16 slices; field of view (FOV) = 256 × 256 × 160 mm; TR/TE = 800/20 ms. Both symmetric (symmetry time $\tau_{sym} = 0$) and asymmetric (asymmetry time $\tau_{asym} = 2.5$ ms) acquisitions are performed in an interleaved approach. The effects of chemical shift are reduced with the asymmetry time difference ($\tau_{asym} - \tau_{sym}$) set to 2.5 ms, equal to one period of the water and lipid chemical-shift difference at 3 T. By opting for a spin-echo (Prammer *et al.*, 1988) rather than a faster gradient echo acquisition (Ericsson *et al.*, 1995; Webb and Macovski, 1991; Schneider and Glover, 1991; Wen and Jaffer, 1995) the sensitivity of the phase unwrapping algorithm to errors is reduced. The acquisition is still sensitive to eddy current effects, which have been found to be small on our system, and image distortion, which is less than 0.2 voxels within the brain.

Each shim coil basis function had been previously calculated *in vivo,* as described in Appendix B. The reference head image was acquired from a single representative volunteer lying in a typical position in the magnet using the same pulse sequence as employed in the brain shim.

Seven normal volunteers were scanned (four male, three female, mean age 30 ± 5 years), each having given informed consent. Scanning was performed in compliance with local ethical committee requirements.

Global Shimming

Three global shimming approaches were used for each volunteer: (1) a "manual" shim, in which the experienced operator manually maximised the FID signal from a simple pulse-acquire sequence utilizing all available shim terms; (2) a brain shim, as presented; (3) a "head" shim, identical to the brain shim except that the brain segmentation step is replaced by magnitude thresholding of the image at 10%. For the manual shim a line width below 30 Hz was deemed acceptable for our system with a maximum shim time of 8 min. The starting shim conditions for each shim approach were equal to a set of average optimized shim currents calculated from a previous group of 45 subjects. As more shim sets are acquired, the starting shim conditions can be continually updated.

Following each shim procedure, a B_0 map was also acquired with the following parameters: data matrix = 64 × 64, 25 axial slices; FOV= 256 × 256 × 150 mm; TR/TE = 1250/20 ms; $\tau = 2.5$ ms. Pre- and postshim water line widths, defined as full width at half-maximum, were measured. For each subject, the postshim B_0 maps were coregistered and masked with a single manually defined brain mask. From these maps values for L and D were calculated. L_{min}, the theoretical minimum value of L, is also calculated following removal of all residual first- and second-order spherical harmonic terms from the brain B_0 map. The measure ($L - L_{min}$) therefore represents the ability of the algorithm to achieve the theoretical minimum value. The significance of improvements in ($L - L_{min}$) were calculated through a paired t test.

Local Shimming

For some studies where only a particular brain region is of primary interest (e.g., a study of frontal lobe function), a localized shimming routine will provide a higher shim uniformity in that region than a global brain shim. In order to investigate the usefulness of weighting the shim target function to each of the particular brain ROIs shown in Fig. 2 (e.g., inferior frontal), a number of studies were made in which each ROI in turn was preferentially weighted. Specifically, for each ROI in turn a weighting of unity was applied, with zero being applied to all remaining brain ROIs. This was conducted in three volunteers, resulting in three data sets per brain ROI. The results of the local shim were compared with a brain shim in order to assess whether the local shim provided a significantly improved B_0 field inhomogeneity in its target region. This assessment was made using measured B_0 maps, masked according to region, that were collected following both the local and the brain shim routines. Within each targeted region the L and D homogeneity measures were made.

Olfactory fMRI Task

The fully automated local shim and brain shim techniques described above were applied in an olfactory fMRI experiment. A continuous air-flow olfactometer was used to deliver a given odorant for a period of 8 s followed by a 24-s delivery of pure air (control condition). The intensity of each odor delivery was rated by the subject through use of a two-button response box on an on-screen scale from −2 (very weak) to +2 (very strong) in increments of 0.25. Six different odors were used (hexanoic acid, octanol, lynalyl acetate, alpha ionone, isovaleric acid, and geranyl acetate at 5% diluted in propylene glycol in the olfactometer) in a randomized block design. A single study consisted of 450 vol of 14 T_2^*-weighted coronal EPI slices. Imaging parameters included TR of 2 s, TE of 25 ms, 64 × 64 data matrix, 192 × 192 mm FOV, 7-mm slice thickness, and readout bandwidth of 100 kHz. Coverage was obtained from +60 mm anterior to −38 mm posterior relative to the anterior commissure.

In this experiment, the orbitofrontal region was of specific interest to the researchers. In addition, the remainder of the brain required sufficient B_0 homogeneity for accurate registration. The olfaction shim was therefore defined as a weighting of 5 units in the inferior frontal ROI and a weighting of unity in the re-

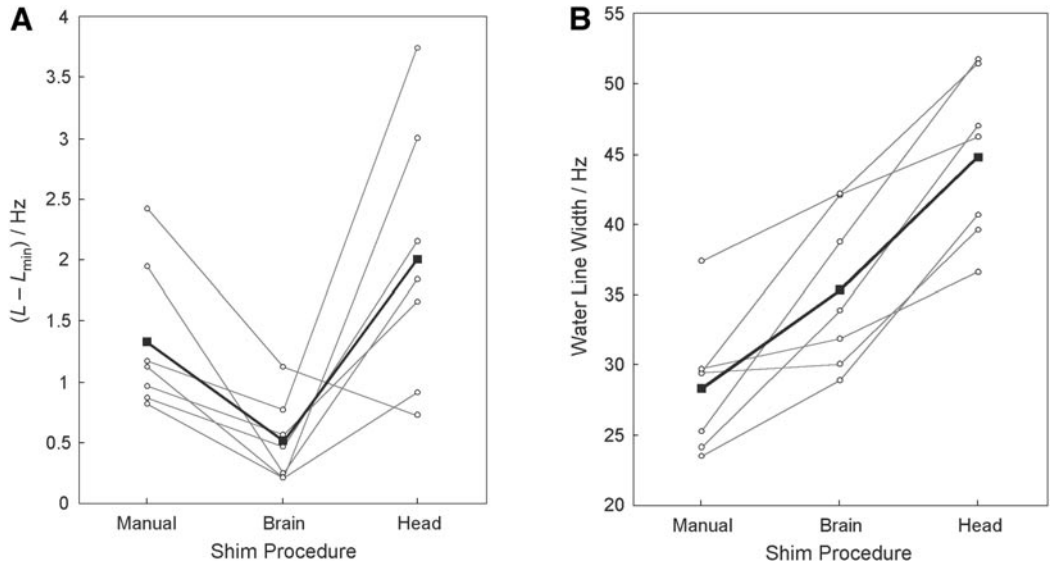

FIG. 3. Postshim B_0 homogeneity measures for the seven volunteers (thin lines) and the mean of all volunteers (thick line) following each shim approach. The three shim methods are defined under Materials and Methods. The measures displayed are (A) the standard deviation of the brain B_0 field, L, relative to L_{min}, the theoretical minimum value of L achievable with the available shim coils, and (B) the water line width defined as full width at half-maximum. The results show that the brain shim produces values of L closest to the theoretical limit. The average absolute value of L_{min} was 20.1 ± 2.5 Hz.

maining four ROIs. This shim specification would be the same for all subjects who might undergo this type of study. The olfaction study was run twice on a single normal subject, the first run following an olfaction shim and the second run following a global shim. Both shims took 80 s and began with the default shim set.

Image preprocessing was performed with FLIRT (Jenkinson and Smith, 2001) for realignment, reslicing with sinc interpolation, and normalization in stereotactic space. SPM99 (Wellcome Institute of Cognitive Neurology, UK) was used to apply spatial smoothing with an 8-mm full width at half-maximum isotropic Gaussian kernel and to carry out global scaling. Time series at each voxel were high-pass filtered (cutoff period 56 s) and low-pass filtered with a hemodynamic response kernel. Statistical parametric maps were generated in SPM99 by fitting a box-car function to each data set convolved with the hemodynamic response function.

RESULTS

Global Shimming

Postshim homogeneity measures after each shim approach are displayed in Fig. 3 for all subjects along with the group mean. Referring to Fig. 3a, the average improvement in $(L - L_{min})$ for the brain shim compared to the manual shim was 59.9 ± 20.8% ($P < 0.05$). The brain shim will, on average, result in a value of L 59.9% closer to the theoretical minimum than the manual shim. For the brain shim compared to the head shim the improvement was 60.8 ± 42.1% ($P < 0.04$). Improvements in the resulting signal loss measure, D, were comparable to improvements in L. As shown in Fig. 3b, the water line width is consistently lower using the manual shim and higher using the head shim. The average run time for a manual shim was $5\frac{1}{2}$ min, while all brain and head shims can be run in under 80 s. The standard deviation in intersubject head tilt (transverse-coronal) was 5°.

Local Shimming

Each local shim can be run in less than 80 s. Average values for L and D across subjects in the five ROIs following global brain shims were: superior frontal 15.5, 9.8 Hz; inferior frontal 28.7, 18.3 Hz; inferior temporal 41.5, 25.3 Hz; cerebellar 19.4, 14.1 Hz; posterior 10.4, 5.2 Hz. This illustrates the different ROI shim characteristics. Figure 4 presents, for each ROI, the average improvement in the local L and D measure following a local shim on that ROI compared to a brain shim. Large average decreases (improvements) in L were found in all ROIs. Improvements in D were also substantial in the superior frontal, inferior frontal, and posterior ROIs, while in the inferior temporal ROI little change was observed. The cerebellum ROI experiences an increased signal loss measure (D) despite an average 21% decrease in L.

Olfactory fMRI Task

Simple effects for each of the odorants were deduced by using the contrast (odor−control). Significant activations in medial orbitofrontal cortex were detected

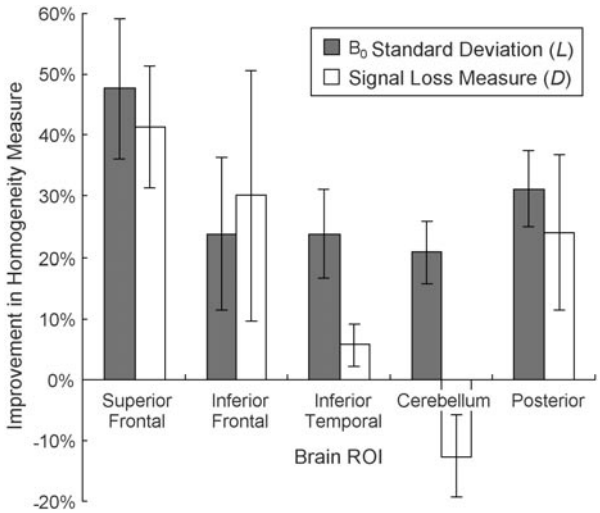

FIG. 4. Improvement in the *L* and *D* homogeneity measures for each of the five brain ROI labels after a local shim on that ROI in comparison to after a brain shim. There are three data points for each ROI. An improvement in *L* represents a reduction in image distortion within the ROI, while an improvement in *D* represents a decrease in local signal loss artifact.

only when using the olfaction shim. An example for one of the odors (hexanoic acid) is shown in Fig. 5 and discussed here. Following the olfaction shim, two significant clusters were found with peaks at $[x, y, z] = [-6, 66, -10]$ and $[x, y, z] = [-6, 40, -26]$ in the normalized Montreal Neurological Institute (MNI) mean brain (Collins *et al.,* 1994) and maximal *Z* scores of 4.35 and 3.58, respectively ($P < 0.001$, uncorrected). When the global shim was performed, no significant activations (at the level chosen of $P < 0.001$, uncorrected) could be detected in any of the inferior frontal regions. These increases in activation levels between the olfaction and global cases correspond to an average 15% increase in baseline EPI signal and 50% decrease in image distortion within the activated area. The maximum variation of B_0 within the activated area decreases from 177 Hz postglobal shim to 141 Hz postolfaction shim.

For the inferior frontal ROI, improvements of 19.3% in *L* and 30.3% in *D* were found postolfaction shim compared to postglobal shim. With reference to Fig. 4, this increase in B_0 homogeneity is typical for the inferior frontal ROI. The resulting reduction in image distortion and signal loss artifacts of the raw EPIs shown in Fig. 5 was therefore representative of a larger sample. The mean odor intensity during the studies, as rated by the subject, were 0.74 for the postolfaction shim and 0.71 for the postglobal shim (paired *t* test, $t = 0.330$, $df = 31$, not significant at $P < 0.5$). There is no significant difference in these intensity means, indicating habituation effects of the subject to the odors were minimal between studies.

DISCUSSION

Global Shimming

The improvement of the brain shim over two widely used and relatively accurate global shim approaches was significant providing brain B_0 standard deviation values that were, on average, within 0.5 Hz of the theoretical minimum. This validates the ability of the brain segmentation step to identify the brain/nonbrain interface for use in both global and local shimming routines.

The three shim approaches can be distinguished by the effective weighting they place on the highly B_0 inhomogeneous inferior brain ROIs. The brain shim provides equal weighting over the entire brain. The manual shim aims to maximize the on-resonance signal from the whole head, weighted by the radiofrequency profile of the coil, as well as to optimize its shape. This results in reduced weighting of the partially off-resonance inferior ROIs. This is evident from the observation that local shimming of the posterior ROI provides line widths similar to those obtained from a manual shim (data not shown). In our study, the manual shim consistently yielded the lowest line width and the head shim the highest line width for each subject, as shown in Fig. 3b. Prammer *et al.* (1988) showed that minimizing *L* also maximises FID signal only if $(B_0 - \langle B_0 \rangle)$ is sufficiently small at all points. These results indicate that this is not true within the human brain—the water line width is not a suitable measure of global brain B_0 homogeneity.

The head shim effectively places increased weighting in the inferior ROIs due to the extension of B_0 inhomogeneous regions into extrabrain tissue, resulting in larger values for all homogeneity measures. However, the head shim improved on the brain shim for one subject. This subject exhibited an unusually large variation of B_0 outside of the three major inhomogeneities and suffered from substandard brain segmentation.

Brain shims were run three times on one volunteer, within a single session, to verify the consistency of the brain shim technique, each run beginning with the

FIG. 5. An example of the contrast (odor−control) for hexanoic acid. A single coronal slice containing the orbitofrontal cortex is shown with contrast activations superimposed following (A) a global shim and (B) an olfaction shim. The activation visible in (B) has a cluster size of 259 voxels with the peak at $[x, y, z] = [-6, 40, -26]$ and a maximum *z* score of 4.35 ($P < 0.0001$, uncorrected). No activations in the orbitofrontal cortex reached this significance after application of the global shim. Corresponding B_0 maps of the brain obtained postglobal shim and postolfaction shim are displayed in (C) and (D), respectively. Sagittal B_0 maps obtained postglobal shim and postolfaction shim are displayed in (E) and (F), respectively. The B_0 range is −100 Hz (white) to 100 Hz (black). In each image, the red cross-hair indicates the location of the activation peak in (B).

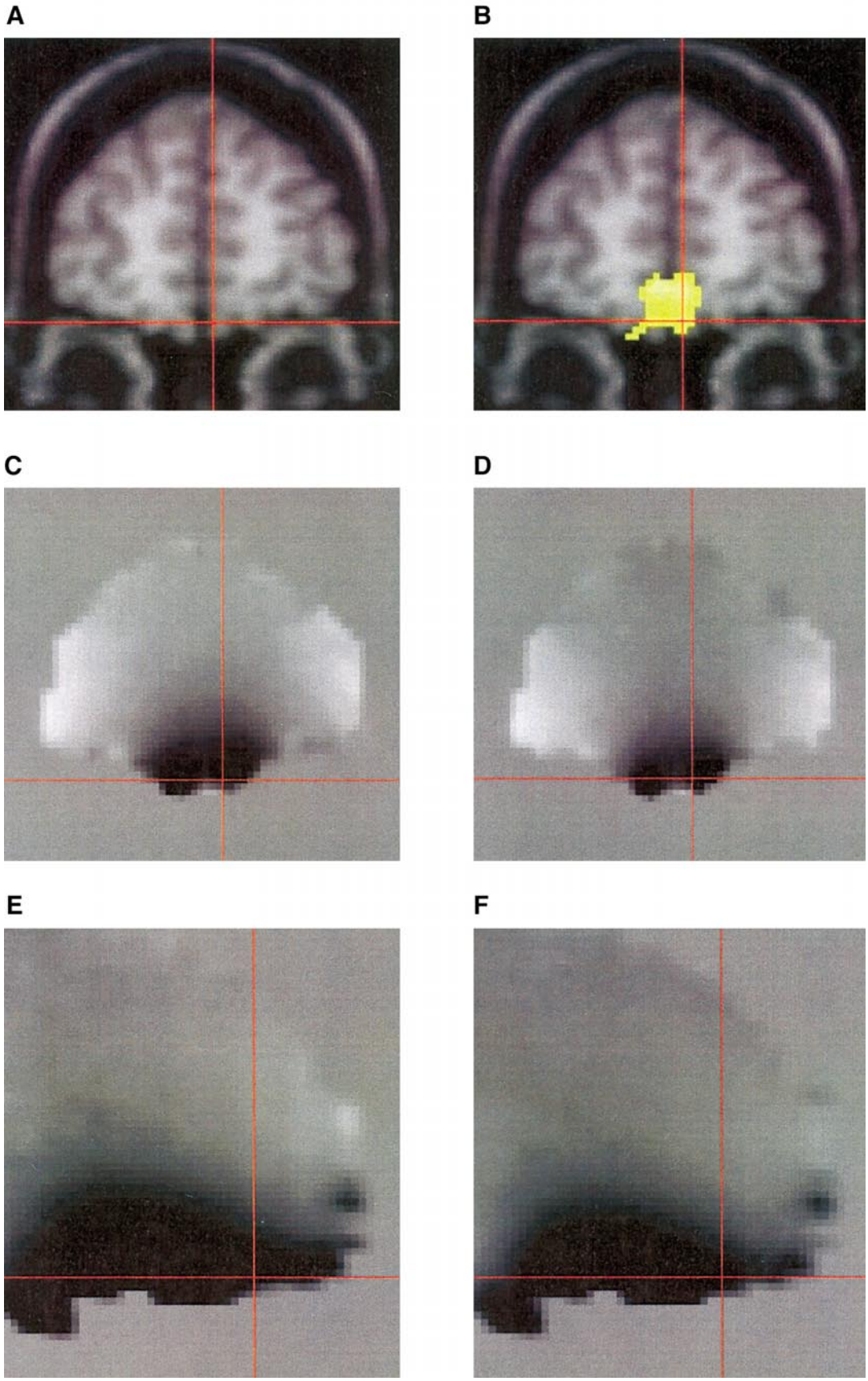
A
B
C
D
E
F

default shim set. The volunteer was removed from the magnet bore and then replaced between runs. The resultant measures for L were 17.8 ± 0.4 Hz.

A single iteration of the global shim was found to be sufficient for almost all experimental needs, producing a range of ($L - L_{min}$) from 0.2 to 1.1 Hz—see Fig. 3a. A second iteration reduced ($L - L_{min}$) to below 0.4 Hz for almost all subjects. Large amounts of head movement during a prolonged imaging session may warrant further intrasession shim runs.

Local Shimming

Local brain shimming on single specified brain ROIs is accurate and reliable, producing large improvements in the target function measure for each brain region. The concurrent reduction in signal loss artifact was ROI-dependent. It should be noted that by distributing weights between ROIs, the resultant B_0 field within the brain can be tailored to meet other experimental preferences.

If the B_0 distribution within an ROI is well approximated by low-amplitude first- and second-order spherical harmonics alone, then the B_0 homogeneity, as measured by L or D, can be significantly improved with the proposed technique. This is typically true of the superior frontal ROI, the posterior ROI, and, to a lesser extent, the inferior frontal ROI. Within the inferior temporal ROI the main B_0 inhomogeneities are of higher spatial frequency, resulting in insufficient characterization with the available shim terms and poor correlation between the L and D measures. The cerebellar ROI contains large B_0 gradients near the outer surface of the structure but low spatial frequency B_0 variation throughout the central region, resulting in the largest D/L ratio of all brain ROIs. The reduction of image distortion in the cerebellum is substantial following a local shim but results in a slight increase in the (relatively small) amount of local signal loss artifact.

Olfactory fMRI Task

Shimming techniques are particularly important in BOLD fMRI experiments in which stimuli are known to elicit activity in brain areas vulnerable to susceptibility artifacts. This is especially true for olfactory stimuli and other experiments involving the orbitofrontal cortex. We show here that performing the olfaction shim (a local shim with weighted specification of the regions of interest, focusing on the inferior frontal ROI) greatly improves signal detection for this particular case, without adding to the duration of the study.

Experiments in non-human primates have shown olfactory areas in the posterior orbitofrontal cortex (Tanabe *et al.*, 1975) and have also shown direct connections from the primary olfactory area to the orbitofrontal cortex terminating in agranular insular transition cortex and a caudomedial part of area 13 (Carmichael *et al.*, 1994). It has been suggested that this region constitutes the secondary olfactory cortex (Rolls, 1997). These regions of the orbitofrontal cortex are likely to have human homologues and it remains an important scientific task to reliably identify these with neuroimaging. The presented technique opens the possibility that regions like the human orbitofrontal cortex can be investigated in high-field fMRI experiments with minimal need for skilled intervention.

General Issues

Experimental limitations to the brain shim method exist. First, slight shim coil nonlinearities can result in suboptimal operation. In addition, postshim head movements imply that brain B_0 homogeneity will slowly worsen over time (Jezzard and Clare, 1999)—the same for all shimming routines.

The ability of the affine transformation to adequately register subjects of differing head size and shape to the reference head set is limited, as are all linear intersubject registration algorithms (Lester and Arridge, 1999). The results of this study support the use of linear registration to construct an *in vivo* brain mask, S_B, but the number of subjects used is relatively low. To confirm the robustness of the brain segmentation step, S_B was compared to a manually defined brain mask for each of the 7 subjects used in this study. The percentage of incorrectly labeled voxels was measured and compared to similarly obtained results from a larger cohort of 40 distinct subjects. The difference in neither the variance nor the mean of the two samples was found to be significant (variance ratio test: $P = 0.30$, $df = 6, 39$; independent two-sample t test: $P = 0.64$, $df = 45$). We therefore conclude that the use of linear registration to construct an *in vivo* brain mask is validated within the larger sample of 40 subjects. However, the brain segmentation step is limited to heads devoid of gross pathology (minor brain pathology, as observed for example in stroke and multiple sclerosis patients, does not significantly impact the quality of registration). For particular subject groups, e.g., pediatric, robust results may be generated through use of a group-specific reference set.

With regard to alternative methods of B_0 field mapping, acquiring phase information along a number of 1-D projections within an operator-defined spherical ROI (Gruetter, 1993) allows for faster shimming but results in suboptimal brain B_0 homogeneity due to the nonspherical and magnetically heterogeneous nature of the head. Our own studies have found the accuracy of EPI B_0 mapping techniques (Reese *et al.*, 1995) at 3 T to be limited.

We find that the low-resolution B_0 maps utilized can adequately model first- and second-order shim terms: a twofold increase in resolution was found to increase the improvement in L for the brain shim versus the man-

ual shim only by approximately 5%. Employing D as the homogeneity target function provides results similar to those presented. More effective reduction of local signal loss artifact requires a smaller specified ROI, higher order shim terms, or dynamic shimming (Blamire *et al.*, 1996) to resolve spatial derivatives of brain B_0 inhomogeneities to a satisfactory degree.

Our simulation studies have shown that certain third-order shim coils, namely z^3, z^2y, and $z(x^2 - y^2)$, would be beneficial for global and local brain shimming. These extra terms, if available, could be simply integrated within the brain shim procedure. We are in the process of incorporating dynamic linear shimming (Blamire *et al.*, 1996) within the brain shim approach. Our second-order shim coils possess settling time constants of between 300 and 1200 ms, making dynamic quadratic shimming problematic on our system. Further techniques to mitigate the effects of higher order spatial frequency B_0 components exist, including optimization of EPI parameters (Ojemann *et al.*, 1997; Merboldt *et al.*, 2000), postacquisition correction of image distortion (Jezzard and Balaban, 1995), z-shimming (Frahm *et al.*, 1988; Constable and Spencer, 1999), and radiofrequency pulse tailoring (Stenger *et al.*, 2000). Calculation of the regional variation of susceptibility artifacts within an echo planar image can also be performed (Lipschutz *et al.*, 2000).

In summary, we have presented a fully automated, accurate and reliable shimming technique that optimizes the B_0 homogeneity of the brain, either globally or locally, and consumes less than 80 s. Automated local shimming is operator-independent and effective with ROI-specific improvements. Preferential weighting of the five ROIs allows the researcher to utilize the full potential of the available shim coils to minimize B_0 inhomogeneity to match the needs of their experiment. The effectiveness of the technique in studies of the orbitofrontal cortex was demonstrated. This brain shim routine is used as standard at our center with robust and successful results.

APPENDIX A

The intersubject variation in major B_0 inhomogeneity position was measured within a distinct group of nine normal subjects (four male, five female, mean age 27 ± 4 years) to validate the use of a single set of brain ROIs. B_0 maps (64×64 resolution, 25 slices) were obtained from each subject following a brain shim and were coregistered using the magnitude-reconstructed B_0 map data. Subject-specific masks for the three major B_0 inhomogeneities (inferior frontal, left inferior temporal, and right inferior temporal) were generated (see below) and separately applied to the registered field maps. The centroid position and maximum B_0 offset of each inhomogeneity was calculated.

The single subject-specific shim masks for the three major B_0 inhomogeneous regions were generated by thresholding the spatial derivative of the field maps in the through-plane (z) direction at 20 Hz cm^{-1}—equivalent to a 20% loss of signal for a 6-mm slice thickness, and assuming only a dependency on intravoxel dephasing in the through-plane direction that is linear. Manually defined brain masks were subsequently applied to exclude nonbrain areas. Each major inhomogeneity, clearly separated within the brain, was labeled to produce the three individual masks for each subject.

TABLE A1

Intersubject Standard Deviation (SD) in the Magnitude (Off-Resonance Frequency) and Location of the Three Major Brain B_0 Inhomogeneities for a Nine Subject Sample

	Maximum amplitude/Hz		SD in centroid location/mm		
B_0 inhomogeneity	Mean	SD	x	y	z
Inferior frontal	−237	43	1.3	4.1	3.0
Left inferior temporal	−139	37	2.0	3.0	3.2
Right inferior temporal	−146	39	1.8	3.0	3.0

The results from this study are presented in Table A1. The greatest variation in position is in the anterior–posterior direction for the inferior frontal inhomogeneity and is indicative of the variation in relative size of the ethmoid and sphenoid sinuses. Despite the small variation in location of the B_0 inhomogeneities, typically 3 mm, the amplitude varies by up to 27%, illustrating the need for subject-by-subject shimming of the brain.

APPENDIX B

The basis function, signifying the strength and spatial variation, of each shim coil was derived as a sum of polynomials up to third order. The same subject that provided the reference head data set was used for shim coil calibration.

The same B_0 field mapping sequence was used as in the brain shim method. A baseline field map was acquired with the brain of the subject optimally shimmed manually. A known current (DAC value offset) was applied to a specific shim coil and another field map acquired. For a given shim coil term, the B_0 variation was calculated as the difference between baseline and offset field maps. In this manner, B_0 inhomogeneities caused by the subject were subtracted out. Polynomials up to third order were fitted to the resulting shim coil field map using a least-squares algorithm. Only those polynomials that significantly reduced the residual B_0 field variation were included in the shim coil basis function. Another set of baseline and current offset B_0 maps was obtained and analyzed with the coil current flowing in the opposite sense and the average shim coil basis function and its amplitude were stored on disk. This procedure was then repeated for the remaining shim coils.

Only the z^2 shim basis function included a significant contribution from a nontheoretical component ($[z^2 - 0.5(x^2 + y^2) - 10z]$ rather than $[z^2 - 0.5(x^2 + y^2)]$). No significant third-order variation was found in any shim coil.

ACKNOWLEDGMENTS

We thank Dr. Han Wen for the original field construction and optimization code. We also gratefully acknowledge financial support from the UK Medical Research Council.

REFERENCES

Blamire, A. M., Rothman, A. L., and Nixon, T. 1996. Dynamic shim updating: A new approach towards optimised whole brain shimming. *Mag. Reson. Med.* **36:** 159–165.

Carmichael, S. T., Clugnet, M.-C., and Price, J. L. 1994. Central olfactory connections in the macaque monkey. *J. Comp. Neurol.* **346:** 403–434.

Collins, D., Neelin, P., Peters, T., and Evans, A. 1994. Automatic 3D intersubject registration of MR volumetric data in standardized Talairach space. *J. Comput. Assist. Tomogr.* **18:** 192–205.

Constable, R. T., and Spencer, D. D. 1999. Composite image formation in z-shimmed functional MR imaging. *Magn. Reson. Med.* **42:** 110–117.

Ericsson, A., Weis, J., Hemmingsson, A., Wikström, M., and Sperber, G. O. 1995. Measurements of magnetic field variations in the human brain using a 3D-FT multiple gradient echo technique. *Magn. Reson. Med.* **33:** 171–177.

Frahm, J., Merboldt, K. D., and Hanicke, W. 1988. Direct FLASH MR imaging of magnetic field inhomogeneities by gradient compensation. *Magn. Reson. Med.* **6:** 474–480.

Gruetter, R. 1993. Automatic, localised in vivo adjustment of all first- and second-order shim coils. *Magn. Reson. Med.* **29:** 804–811.

Holz, D., Jensen, D., Proksa, R., Tochtrop, M., and Vollmann, W. 1988. Automatic shimming for localised spectroscopy. *Medical Physics* **15:** 898–903.

Hu, J., Javaid, T., Arias-Mendoza, F., Liu, Z., McNamara, R., and Brown, T. R. 1995. A fast, reliable, automatic shimming procedure using ^{1}H chemical-shift-imaging spectroscopy. *J. Magn. Reson. B* **108:** 213–219.

Jenkinson, M., and Smith, S. 2001. A global optimisation method for robust affine registration of brain images. *Medical Image Analysis* **5:** 143–156.

Jezzard, P., and Balaban, R. S. 1995. Correction for geometric distortion in echo planar images from B_0 field variations. *Magn. Reson. Med.* **34:** 65–73.

Jezzard, P., and Clare, S. 1999. Sources of distortion in functional MRI data. *Human Brain Mapping* **8:** 80–85.

Lester, H., and Arridge, S. R. 1999. A survey of hierarchical nonlinear medical image registration. *Pattern Recogn.* **32:** 129–149.

Li, S., Dardzinski, B. J., Collins, C. M., Yang, Q. X., and Smith, M. B. 1996. Three-dimensional mapping of the static magnetic field inside the human head. *Magn. Reson. Med.* **36:** 705–714.

Lipschutz, B., Ashburber, J., Friston, K., and Price, C. 2000. Assessing study-specific regional variation in fMRI signal. *NeuroImage* **13:** 392–398, doi:10.1006/nimg.2000.0687.

Mackenzie, I. S., Robinson, E. M., Wells, A. N., and Wood, B. 1987. A simple field map for shimming. *Magn. Reson. Med.* **5:** 262–268.

Merboldt, K., Finsterbusch, J., and Frahm, J. 2000. Reducing inhomogeneity artifacts in functional MRI of human brain activation—Thin sections vs gradient compensation. *J. Magn. Reson.* **145:** 184–191.

Nelder, J. A., and Mead, R. 1965. A simplex method for function minimization. *Comput. J.* **7:** 308–313.

Ojemann, J. G., Akbudak, E., Snyder, A. Z., McKinstry, R. C., Raichle, M. E., and Conturo, T. E. 1997. Anatomic localization and quantitative analysis of gradient refocused echo-planar fMRI susceptibility artifacts. *NeuroImage* **6:** 156–167, doi:10.1006/nimg.1997.0289.

Prammer, M. G., Haselgrove, J. C., Shinnar, M., and Leigh, J. S. 1988. A new approach to automatic shimming. *J. Magn. Reson.* **77:** 40–52.

Reese, T. G., Davis, T. L., and Weisskoff, R. M. 1995. Automated shimming at 1.5T using echo-planar image frequency maps. *J. Magn. Reson. Imaging* **5:** 739–745.

Rolls, E. T. 1997. Taste and olfactory processing in the brain and its relation to the control of eating. *Crit. Rev. Neurobiol.* **11:** 263–287.

Schneider, E., and Glover, G. 1991. Rapid in vivo proton shimming. *Magn. Reson. Med.* **18:** 335–347.

Spielman, D. M., Adalsteinsson, E., and Lim, K. O. 1998. Quantitative assessment of improved homogeneity using higher-order shims for spectroscopic imaging of the brain. *Magn. Reson. Med.* **40:** 376–382.

Stenger, V. A., Boada, F. E., and Noll, D. C. 2000. Three-dimensional tailored RF pulses for the reduction of susceptibility artifacts in T_2*-weighted functional MRI. *Magn. Reson. Med.* **44:** 525–531.

Tanabe, T., Yarita, H., Iino, M., Ooshima, Y., and Takagi, S. F. 1975. An olfactory projection area in orbitofrontal cortex of the money. *J. Neurophysiol.* **38:** 1269–1283.

Tropp, J., Derby, K. A., and Hawryszko, C. 1989. Automated shimming of B_0 for spectroscopic imaging. *J. Magn. Reson.* **85:** 244–254.

Webb, P., and Macovski, A. 1991. Rapid, fully automatic, arbitrary-volume *in vivo* shimming. *Magn. Reson. Med.* **20:** 113–122.

Wen, H., and Jaffer, F. A. 1995. An in vivo automated shimming method taking into account shim current constraints. *Magn. Reson. Med.* **34:** 898–904.